193 nm STEP AND SCAN LITHOGRAPHY

Guy Davies, Judon Stoeldraijer, Barbra Heskamp, Jan Mulkens, Joost Sytsma, Hans Bakker
ASML BV, De Run 1110, 5503 LA Veldhoven, The Netherlands

Holger Glatzel, Christian Wagner, Oliver Roempp, Rainer Boerret
Carl Zeiss, D-73446 Oberkochen, Germany

This paper was first presented at the
SEMI Technology Symposium 98, Makuhari Messe, Chiba, Japan

193 nm STEP AND SCAN LITHOGRAPHY

Guy Davies, Judon Stoeldraijer, Barbra Heskamp, Jan Mulkens, Joost Sytsma, Hans Bakker
ASML BV, De Run 1110, 5503 LA Veldhoven, The Netherlands

Holger Glatzel, Christian Wagner, Oliver Roempp, Rainer Boerret
Carl Zeiss, D-73446 Oberkochen, Germany

ABSTRACT

This paper presents the ASML PAS 5500/900 full field Step & Scan system, intended for pilot and process development. The performance of the Illumination and Projection subsystems is discussed, as are issues concerning the entire system (including imaging, overlay and throughput). The system's performance, using different resist systems, will be presented and compared.

1. INTRODUCTION

The ever-increasing march down the Semiconductor Industry Association's (SIA) roadmap requires improvements in resolution that can only be met by exposing with light of smaller wavelengths. 193 nm lithography equipment is the next generation of exposure tools that will be introduced into production. At this time, full field process development systems are being introduced into the market to meet the need for early 193 nm pilot and process development. These systems will be of the Step & Scan variety, to meet the need for full field matching to the current and future generations of high numerical aperture (NA) deep UV Step & Scan systems.

The introduction point of 193 nm lithography is closely related to the fortunes of 248 nm. We have seen that 248 nm exposure tools were introduced at 0.25 μm and have been pushed to 0.18 μm. Further developments at 248 nm will occur as high NA (> 0.6) DUV systems are introduced into the market place. These systems will allow 0.15 μm production and possible development work at the 0.13 μm technology node.

Lithography at 193 nm will be introduced at 0.15 μm before moving swiftly on to the 0.13 μm node, where its use will probably peak. There are many developments such as phase shift masks and quadrapole illumination that may push 193 nm on towards 0.10 μm and possibly beyond.

The relative cost of ownership of each system will be one of the main driving forces to the introduction of 193 nm lithography, in other words 'when do the costs associated with contrast enhanced 248 nm lithography make it more expensive than 193 nm lithography'. Current expectations are that early 193 nm tools, such as the PAS 5500/900, will be used for pilot production and as learning tools for the issues relating to 193 nm production, especially those relating to photoresists and other process issues.

The developments of 193 nm systems have required large investments in areas such as lasers, lens design, photoresist and raw materials such as calcium fluoride and quartz. These technological developments have been presented in other publications. Parallel developments in these areas have allowed ASML to develop a full field 193 nm Step & Scan exposure system known as the PAS 5500/900. In this paper we shall discuss some of the design issues relating to this system, including laser, illuminator and lens. Results will be presented showing static and full field performance of the various subsystems, along with imaging results.

193 nm lithography will be expensive owing to laser costs, optical damage, photoresist and reticle costs. The effect of these and other parameters will also be discussed in the context of pilot 193 nm lithography and as a complimentary technique to high NA DUV lithography.

2. GENERAL SYSTEM DESCRIPTION

The PAS 5500/900 is based upon the body of the PAS 5500/500, a DUV Step & Scan system. Several major changes have been made to the PAS 5500/500, including:

- the STARLITH 900 lens, which is a 4X reducing projection lens with an NA of 0.60 to 0.45,
- the AERIAL II illuminator,
- a nitrogen purged optical column.

The AERIAL II illuminator is a modification of the basic AERIAL illuminator which contains calcium fluoride elements to reduce the effect of compaction and induced absorption seen in quartz optical elements with high fluence values.

The system is capable of using either Cymer or Lambda Physik lasers, these are line-narrowed (0.7 picometer) systems, suitable for use with a refractive lens design.

Several incremental improvements have been added such as off-axis alignment, Transmission Image Sensor, an advanced grey filter and a wafer stage optimized for the speed of current and future 193 nm photoresists. Table 1 lists the specifications of the system.

Both the Transmission Image Sensor and the advanced grey filter are necessary to cope with potential drift caused by changing material behavior.

Table 1 PAS 5500/900 specifications

Item	Specification
Resolution (μm)	≤ 0.15
Field size (mm)	26 x 33
Wavelength (nm)	193.368
Reduction	4X
NA	0.60 - 0.45
Sigma range, conventional	0.35 - 0.85
Sigma range, annular (outer)	0.30 - 0.85
Sigma range, annular (inner)	0.15 - 0.60
CD uniformity at best focus (nm)	22
CD uniformity over ± 0.2 μm focus range (nm)	32
Dynamic distortion (nm)	25
Overlay, single machine (nm)	40
Overlay, matched to PAS 5500/500 (nm)	60
Overlay, matched to PAS 5500/400 (nm)	60
Image plane flatness (IPD) (nm)	200
Astigmatism (nm)	150
Throughput, 32 x 16 mm, 200 mm wafers, 46 shots @ 10 mJ/cm^2 (WPH)	40
Laser 1 kHz, 0.6 pm (W)	5
Dose repeatability (%)	1.5
Uniformity (%)	1.2

3. IMAGING SIMULATION

As with any new tool, extensive simulations have been performed to determine the optimum imaging conditions for a range of feature types and sizes.

All simulations were carried out using Prolith's Lumped Parameter Model (LPM). The LPM model uses a lumped contrast merit function, γ, which incorporates photoresist exposure and development properties.

The simulations tend to be a better approximation than an aerial image model, but are less accurate than a full-scale development model. The trends are, however, fully consistent with more complex models which include photoresist development.

To determine optimum NA/σ combinations, the following three indices were used:

- maximum DoF at 10% exposure latitude,
- optimum CD variability as determined by a Monte Carlo analysis,
- iso-dense bias.

Table 2 shows the optimum NA/s conditions which give the best compromise between DoF, CD uniformity and iso-dense bias. The same conditions appeared to be optimum for a range of differing feature sizes, as were the standard conditions used for the initial experiments on the PAS 5500/900.

Table 2 Optimum NA/σ settings, determined by simulation

	NA	σ
Optimum conventional	0.6	0.85
Optimum annular	0.58	0.8/0.5

4. SUBSYSTEM PERFORMANCE

The results discussed in this section were collected whilst the system was in a 'static' mode. In this way the performance in the slit can be determined, and errors introduced whilst the system is scanning are eliminated.

4.1 Illumination

The design goals for the 193 nm illumination system are threefold:

- to maximize optical efficiency.
- to maximize life time.
- to facilitate AERIAL settings (full range of coherence and annularity).

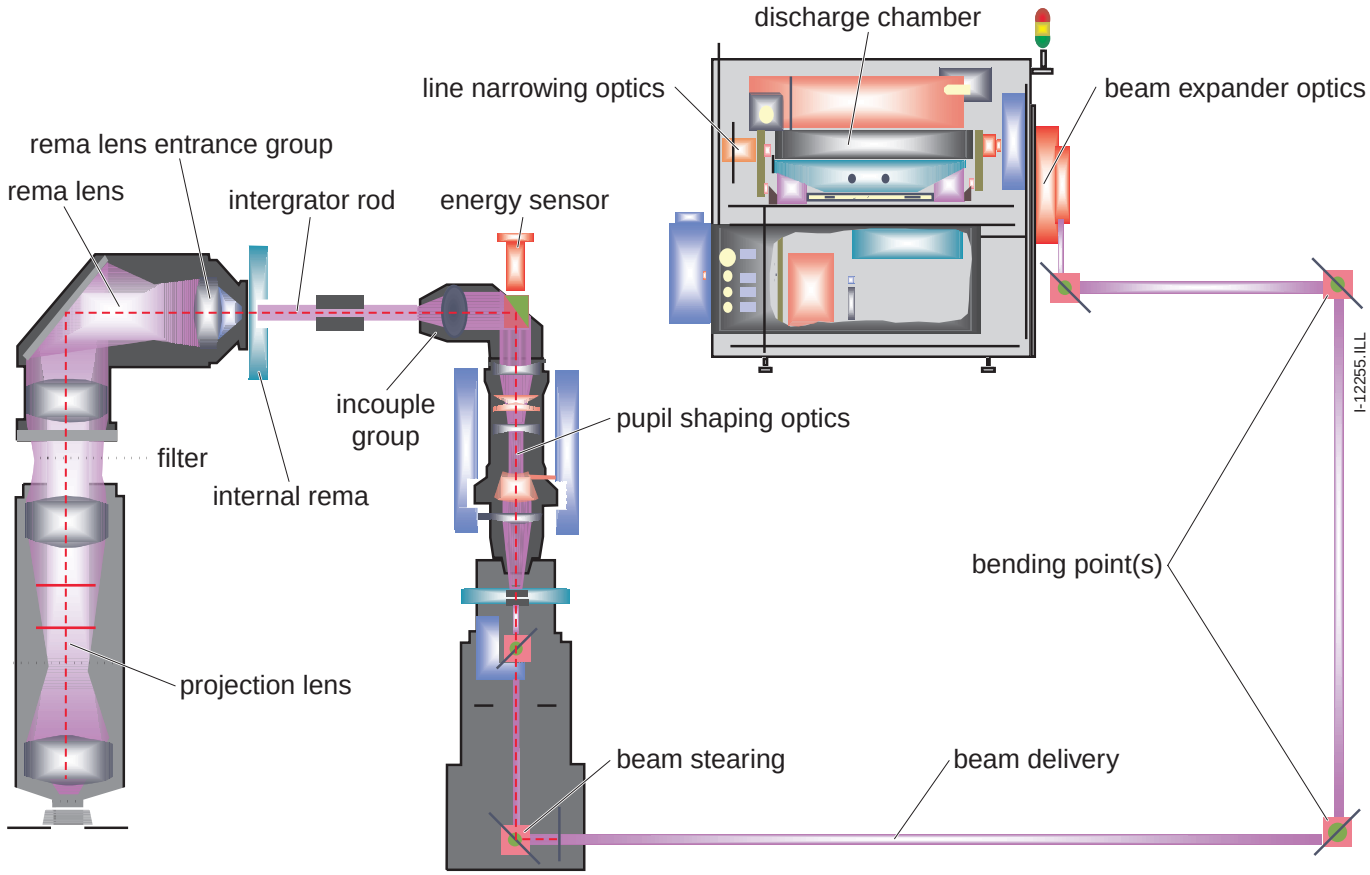

Figure 1 Optical layout of the PAS5500/900 system. Indicated are the optical parts that are replaceable.

The first two design goals are achieved as follows:

- by using improved optical designs with less elements and shorter optical path length in material,
- by the introduction of CaF_2 as the main optical material for the illumination optics,
- by purging the illumination optical path with nitrogen gas.

The third design goal is achieved by 'copying' the optical concept known from the PAS 5500/300 and PAS 5500/500 AERIAL systems.

The general layout of the optical path is presented in Figure 1, which shows that the illumination function is created with the following sub-modules:

- the ArF laser, line-narrowed to < 0.7 pm,
- the beam delivery system, capable of transporting the laser beam over a maximum distance of 20 meters from the laser to the illuminator entrance. The beam delivery system comprises a beam expander, up to five bending points and an automated beam steering system.
- the illumination system, comprising:
  - Pupil Shaping Optics (PSO), to create the partial coherence and flexible annular illumination mode,
  - the energy sensor, integrated in the PSO,
  - the integrator rod, needed for the creation of the slit intensity profile,
  - the internal REticle MAsking (REMA) unit, which allows controlled illumination of selected reticle areas,
  - the REMA lens, which images the created slit and the internal masking blades on to the reticle.

The conventional and annular settings are created in a similar way to the AERIAL illuminators used in the PAS 5500/300 and PAS 5500/500. In the Step & Scan system, the user-defined illumination settings are automatically transferred into the required positions of lens elements in the PSO.

4.1.1 Uniformity

The uniformity is measured at reticle level as a function of NA versus σ setting. The results are shown in Figure 2 and have been summarized in Table 3.

Table 3 Uncorrected maximum measured uniformity at reticle level

Setting	Uniformity (%)
NA = 0.6, σ = 0.85	1.2
NA = 0.58, σ_{inner} = 0.8, σ_{outer} = 0.5	0.8
All others	2.6

Using a symmetrical gradient filter, it is possible to compensate for the symmetrical component in the uniformity. This is done by minimizing the uniformity at one particular setting (NA = 0.6, σ = 0.85). The ensuing correction is then also applied to other settings. The calculated results are presented in Figure 3.

A better correction may be obtained if a dynamic correction is applied. This dynamic correction allows optimization of the uniformity for different NA/σ settings. Across all settings the improvement with the dynamic correction is clear (Figure 4).

We conclude that the uniformity at wafer level can be brought within specifications after applying uniformity correction mechanisms.

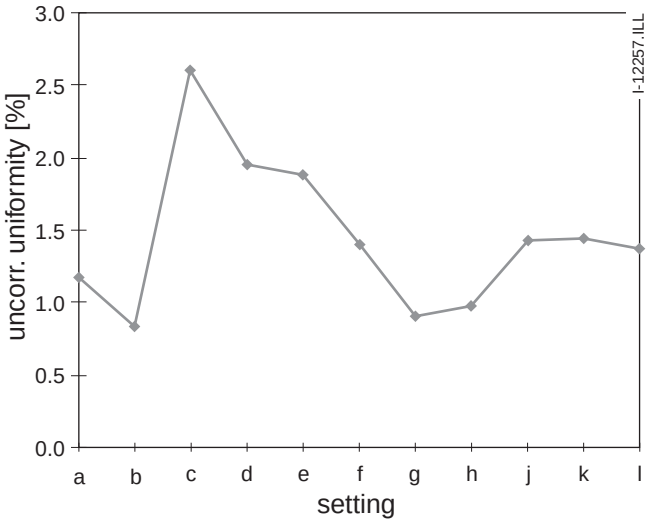

Figure 2 Uniformity across NA/σ range (refer to Table 4)

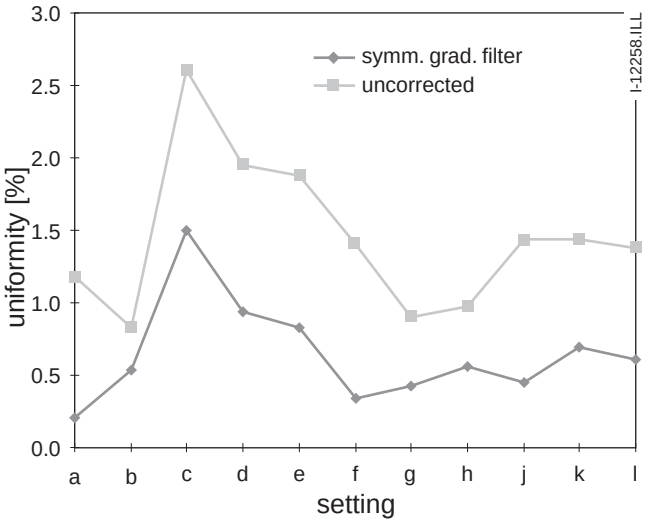

Figure 3 Uniformity before and after simulating application of a radial symmetric gradient filter (refer to Table 4)

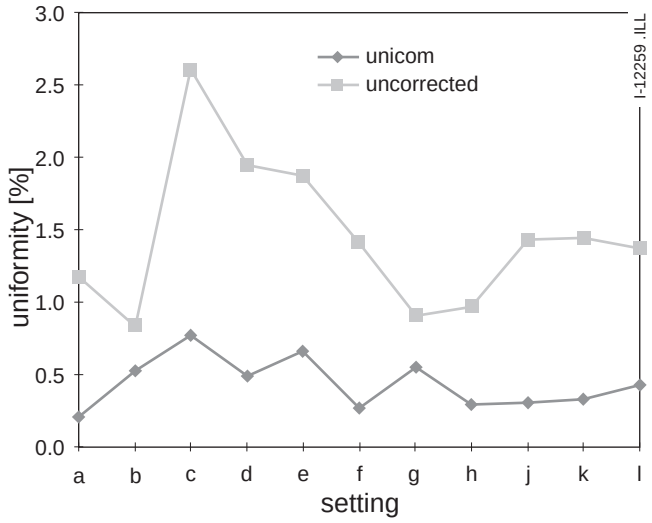

Figure 4 Uniformity before and after simulating application of a uniformity correction mechanism for different NA/s settings (refer to Table 4)

Table 4 Legend for Figure 2, Figure 3 and Figure 4

Setting	NA	σ_{inner}	σ_{outer}
a	0.6	-	0.85
b	0.58	0.8	0.5
c	0.63	0.31	0.102
d	0.63	0.38	0.124
e	0.63	0.45	0.146
f	0.63	0.55	0.178
g	0.63	0.6	0.3
h	0.63	0.75	0.35
j	0.63	0.87	0.278
k	0.63	0.87	0.42
l	0.63	0.87	0.57

4.1.2 Purging performance

The interaction of 193 nm light with oxygen and carbon-hydroxides requires that the system be purged with nitrogen. To ensure that the required nitrogen concentration is reached in a relatively short time, the illuminator is divided into several compartments.

The absorption of 193 nm light by oxygen results in the creation of ozone; this not only drastically reduces the efficiency of the system, but also provides a potential hazard to humans and optics. The safety mechanism which is implemented in the PAS 5500/900 measures the nitrogen overpressure in each of the compartments. A decrease in nitrogen overpressure (indicative of a leak in the system) first leads to a warning and, if no corrective action is taken, eventually to a safety shutdown. This ensures a homogeneous nitrogen atmosphere and prevents oxygen from entering the compartments, and thus the creation of ozone.

Two areas of the optical column that are not purged are the wafer stage and the reticle stage. There are three reasons for this: difficulties in sealing large volumes within the system's existing structure, possible process issues in exposing wafers in a dry nitrogen environment, and enhanced pellicle lifetime in an oxygen-based environment. In these spaces, the ozone concentration is reduced to an acceptable level by increasing the airflows through these spaces.

4.2 Projection system

Measurements were taken of distortion, focal plane and astigmatism in a static mode to determine the contributions of the lens to the overall error budgets. The measurements were exposed using the standard conventional settings with NA = 0.6 and σ = 0.85. Wafers were exposed and measured using the alignment system of the PAS 5500/900. The focal plane and astigmatism measurements were performed using the FOCAL technique with 0.2 μm chops and I-line photoresist TOK ip 3650 was used in the exposure of the wafers at a dose of 100 mJ/cm^2.

In the static mode, the measurements are performed at 13 x 4 locations in the illumination slit of 26 mm x 9 mm. The lens fingerprints for distortion, focal plane and astigmatism are presented in Figures 5, 6 and 7 respectively, and are summarized in Table 5.

Another lens parameter that was investigated was that of straylight, a critical parameter influencing system issues such as CD uniformity. A static straylight test based on the linescan measurement technique was performed. A spot sensor at wafer level is scanned under a nearly open reticle with a 2 mm (at reticle level) wide chrome cross. The amount of straylight is calculated with equation (1), where I equals the ratio of spot sensor over energy sensor intensities.

$$Straylight = \frac{I(clear)}{max(I(dark))} \quad (1)$$

The results for straylight in X and Y directions are shown in Figures 8 and 9. They are comparable with data measured on 248 nm systems.

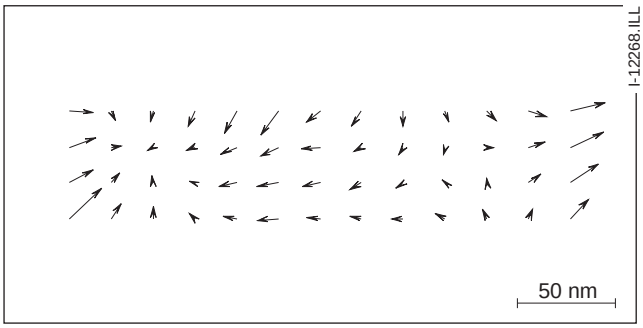

max NCE X/Y = 17.5/15.1 nm

Figure 5 Static lens distortion of the PAS 5500/900 lens, measured over the illumination slit. Maximum vectors XY: 18/15 nm
NA = 0.6, σ = 0.85

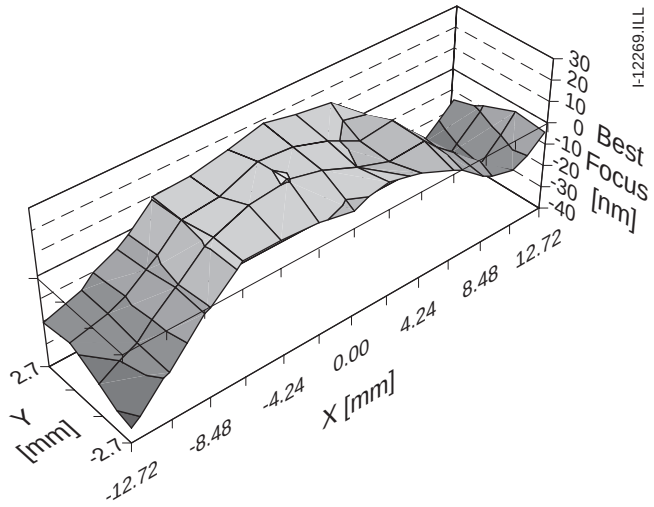

Figure 6 Static focal plane measurement of the PAS 5500/900 lens measured over the illumination slit
NA = 0.6, σ = 0.85

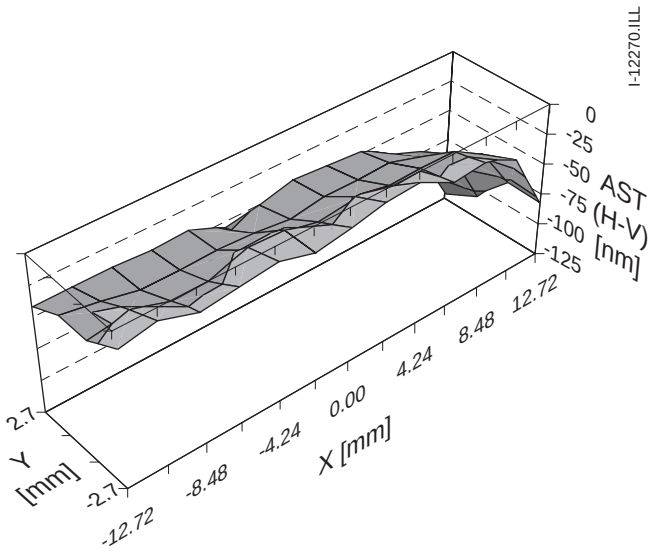

Figure 7 Static astigmatism measurement of the PAS 5500/900 lens measured over the illumination slit
NA = 0.6, σ = 0.85

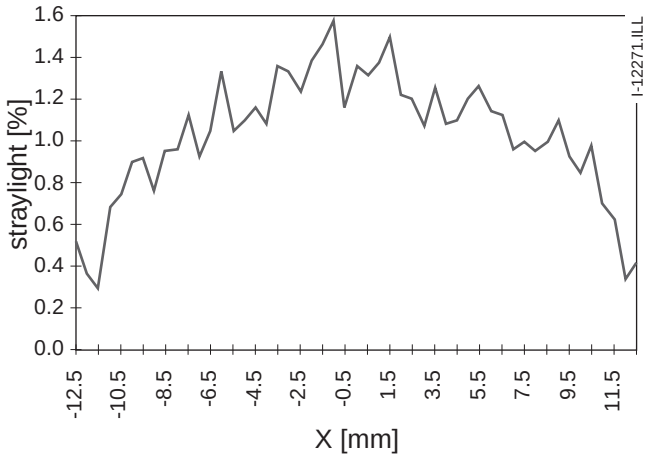

Figure 8 X direction straylight PAS 5500/900
NA = 0.6, σ = 0.85

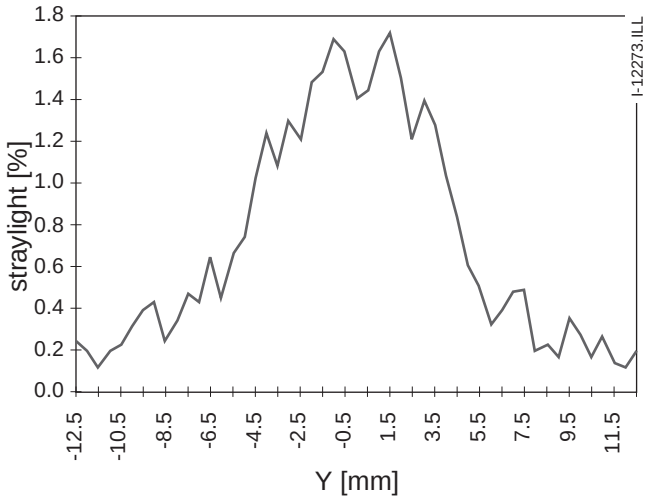

Figure 9 Y direction straylight PAS 5500/900
NA = 0.6, σ = 0.85

Table 5 Summary of static (lens) measurements and dynamic (system) measurements
NA = 0.6, σ = 0.85

	Static	System
Distortion X/Y (nm)	18/15	18/11
FPD/IPD (nm)	122	183
Astigmatism (nm)	122	172

5. SYSTEM PERFORMANCE

The performance of the Step & Scan systems is heavily dependent on overall system integration; the correct functioning of subsystems allows excellent overlay and imaging results to be realized.

The results presented in the following sections are measured whilst the system is scanning and therefore represent production performance.

5.1 Distortion, image plane deviations and overlay

Dynamic measurements are performed at 13 x 19 locations across the 26 mm x 33 mm field. The measurements are corrected for residual dynamically adjustable parameters by means of a least square optimization. This results in the focal plane, system distortion and astigmatism fingerprints shown in Figures 10, 11 and 12. The results have been summarized in Table 5.

Table 6 Summary of maximum difference in distortion for two NA/σ settings

	Maximum difference NCE, from NA = 0.6, σ = 0.85	
	X (nm)	Y (nm)
NA = 0.58, σ_{outer} = 0.8, σ_{inner} = 0.5	9	3
NA = 0.63, σ = 0.35	21	5

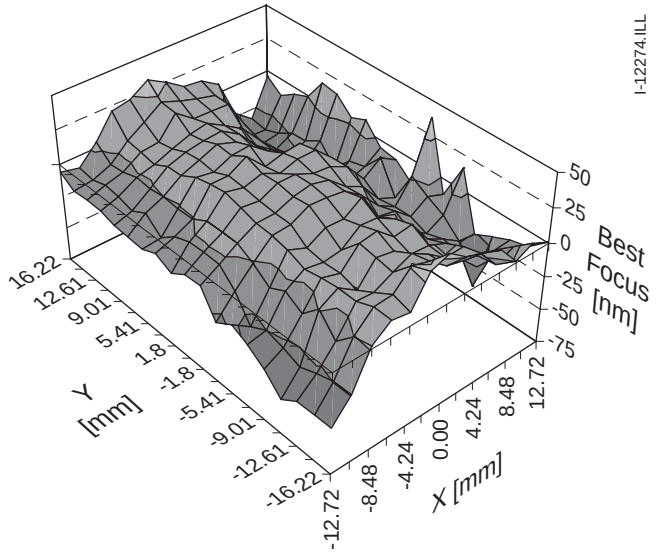

Figure 10 Dynamic image plane deviation measured over the full 26 mm x 33 mm field IPD = 183 nm, NA = 0.6, σ = 0.85

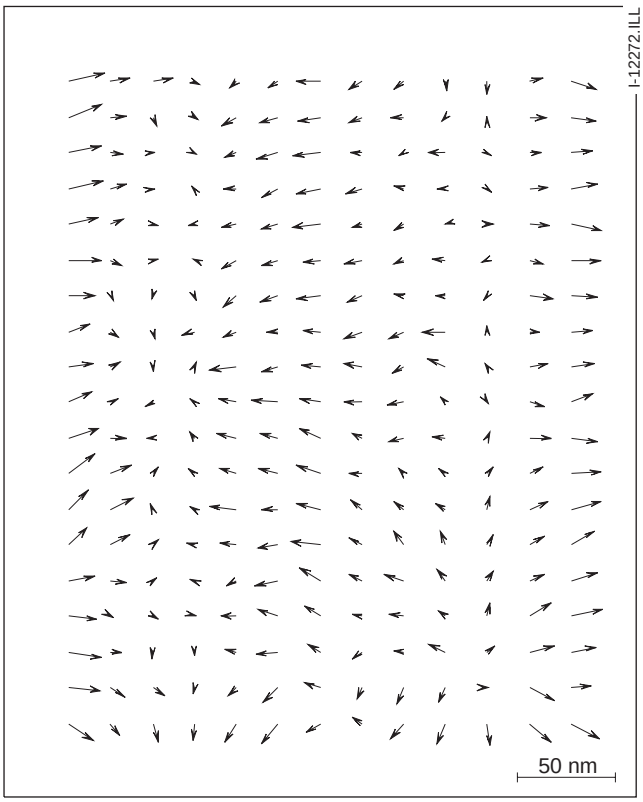

max NCE X/Y = 18/11 nm

Figure 11 Dynamic system distortion of the PAS 5500/900 lens measured over the scanning field. Max vectors X/Y: 18/11 nm NA = 0.6, σ = 0.85

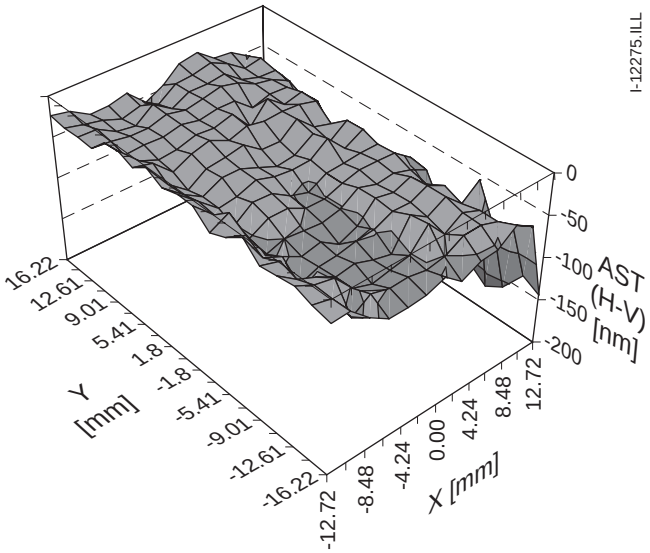

Figure 12 Dynamic astigmatism measured over the full 26 mm x 33 mm field AST=172 ± 28 NA = 0.6, σ = 0.85

Distortion was also determined for other NA/σ combinations, the results are summarized in Table 6. The data shown in this table refers to the maximum difference in Non Correctable Errors (NCE). The reference to which the other two settings are compared are: NA = 0.6, σ = 0.85.

The PAS 5500/900 is a critical-level system that will be used in processes where the majority of levels will be DUV and some i-line. Consequently, the ability to match to DUV and i-line systems is of great importance. The single machine overlay of the PAS 5500/900 was measured and the results for 99.7% of all data are X = 19 nm, Y = 31 nm, as shown in Figure 13.

By modeling datasets, it is possible to obtain an impression of the matching performance of a PAS 5500/900 with a PAS 5500/500. In this case the expected overlay errors are X = 25 nm and Y = 35 nm.

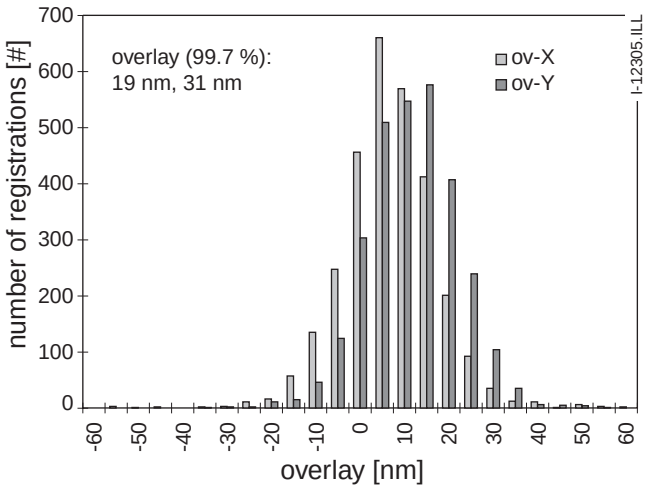

Figure 13 PAS 5500/900 single machine overlay

5.2 Imaging results

The following results were evaluated with a number of differing photoresists which were all processed on a Polaris 2000 wafer track. The specific process conditions are shown in Table 7.

The metrology systems used to measure the exposed wafers were a Hitachi S-7800H diagnostic SEM and a Hitachi S-8C40 top down SEM for inline CD measurements.

The OMM ARCH 410/510 process differs slightly from conventional resist systems, where the top coat (ARCH 410) acts as a mask for the undercoat (ARCH 510), which is then used as the mask system for the underlying layer.

Although the processing complexity is the same as a single layer resist on a BARC, it has the advantage that the imaging is done in a thin film (250 nm) with all the advantages that this encompasses such as improved depth of focus and improved exposure latitudes and resolution.

Table 7 Process conditions for the photoresists used in this paper

	OMM ARCH 410	IBM v2
Thickness	250 nm	280 nm
Soft bake temperature	100 °C	130 °C
Soft bake time	90 s	60 s
PEB temperature	100 °C	140 °C
PEB time	90 s	60 s
Developer type	OPD 262	0.015N TMAH
Develop time	30 s puddle	30 s immersion
BARC/Undercoat	ARCH 510	DUV 30
BARC/Undercoat thickness	500 nm	52 nm

5.3 CD linearity

The system's linearity was evaluated using two resists: OMM ARCH 410/510 and IBM v2. In both cases, similar results were seen with the high NA conventional condition (NA = 0.6, σ = 0.85), showing dense (1:1 lines and spaces) linearity down to 0.15 µm (Figure 14) and isolated linearity down to 0.11 µm (Figure 15).

Cross sections from these data after wet development are shown in Figure 16. The same features, etched into the undercoat, are shown in Figure 17.

Linearity was also determined for other conditions; for conciseness, only the cross sections of a high NA annular condition are shown in Figure 18. As can be expected, the ultimate resolution is improved by the use of this annular condition with isolated linearity approaching 0.10 µm and dense linearity reaching 0.14 µm.

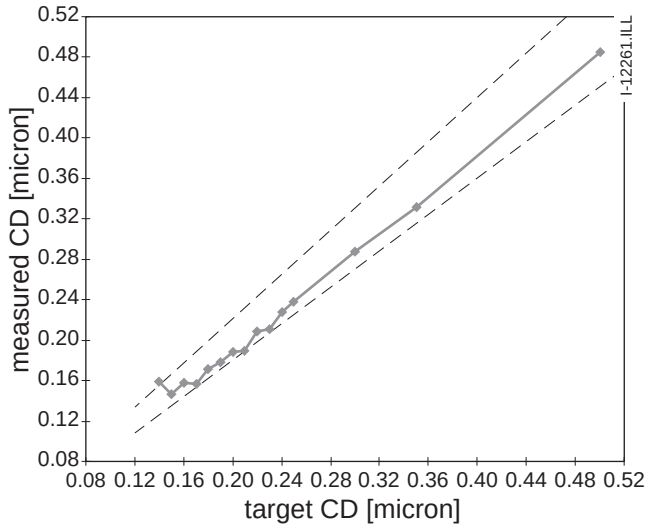

Figure 14 CD linearity of dense lines
NA = 0.6, σ = 0.85, ARCH 410/510 after wet development

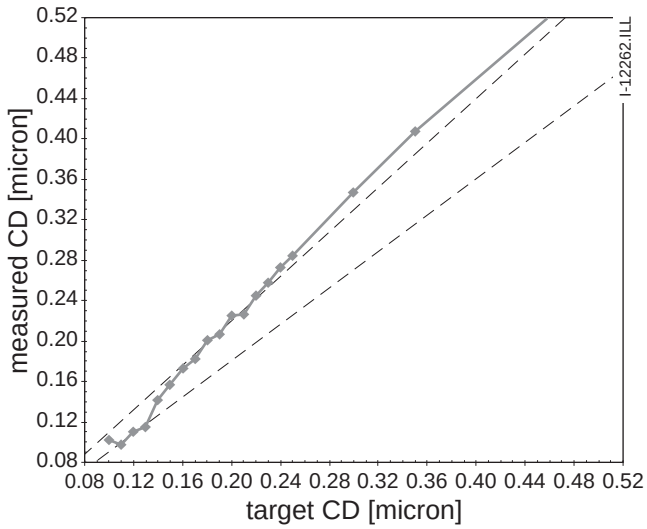

Figure 15 CD linearity of isolated lines
NA = 0.6, σ = 0.85, ARCH 410/510 after wet development

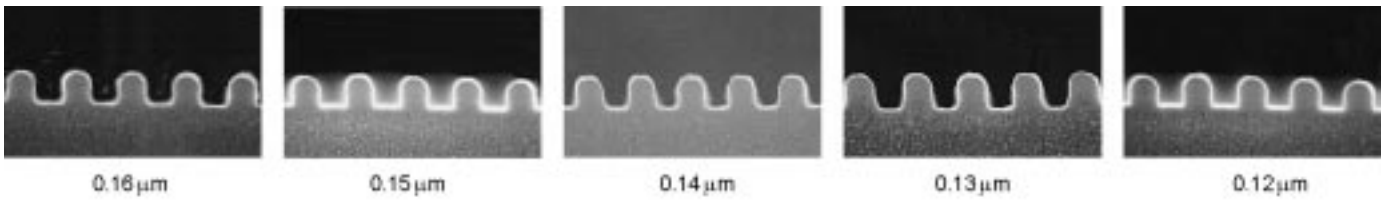

Figure 16 Cross sections of ARCH 410/510 showing linearity of dense lines after wet development
NA = 0.6, σ = 0.85

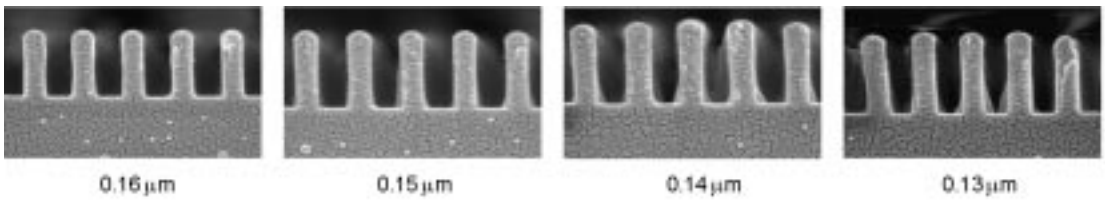

Figure 17 Cross sections of ARCH 410/510 showing linearity of dense lines after dry etch of the bottom layer
NA = 0.6, σ = 0.85

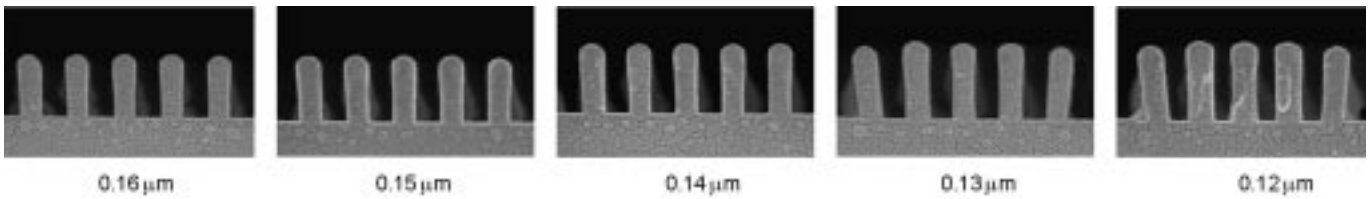

Figure 18 Cross sections of ARCH 410/510 showing linearity of dense lines after dry etch of the bottom layer
NA = 0.63, σ_{outer} = 0.8, σ_{inner} = 0.5

5.4 Pitch linearity

The pitch linearity is an important parameter as it gives the process engineer an understanding of how linewidths of the same nominal CD but differing pitches will print.

Pitch linearity is influenced by several variables, such as the entire photoresist process and optical parameters (such as NA and σ). Where sensitivities to differing pitches are observed, this may indicate that further NA/σ or photoresist optimization is necessary, or that reticle correction through Optical Proximity Correction (OPC) becomes a necessity.

The pitch linearity was evaluated for both the IBM and OMM photoresist processes at a nominal CD of 0.14 µm and is shown in Figures 19 and 20. It appears that, for both processes, a large iso-dense bias is present and that, based on this first data, an optimization of NA and σ conditions is necessary. This effect can also be seen in the results from measurements of process windows as shown in section 5.5.

The differences in nominal CD for the curves shown in Figures 19 and 20 are due to differences in targeting the correct energy for dense or isolated lines. It is the *shape* of the curve which is the important parameter.

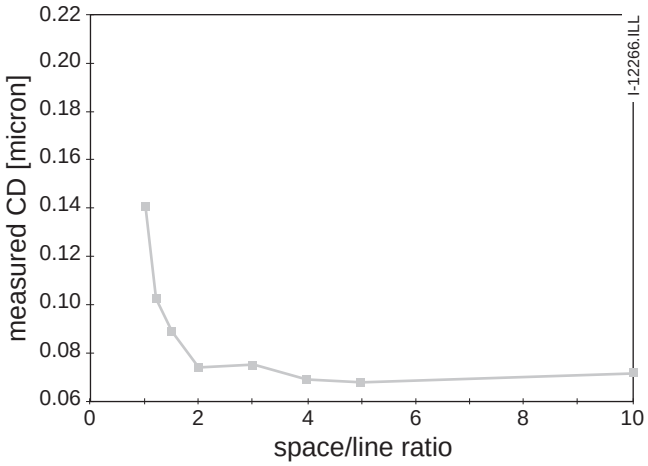

Figure 19 Pitch linearity for 0.14 µm lines
IBM v2 on DUV 30 BARC
NA = 0.58, σ_{outer} = 0.8, σ_{inner} = 0.5

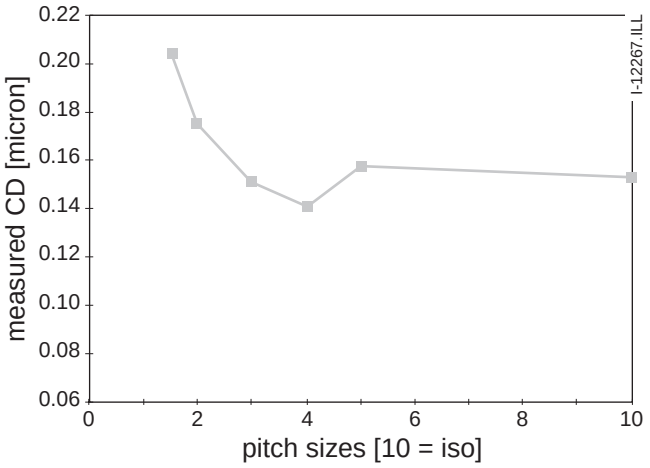

Figure 20 Pitch linearity for 0.14 µm lines
OMM ARCH 410/510 on DUV 30 BARC
NA = 0.58, σ_{outer} = 0.8, σ_{inner} = 0.5

5.5 Process windows

To determine some of the imaging characteristics of the system, the process windows were determined for a variety of CD sizes.

As the raw data in Bossung curve form is hard to analyze in a quantitative form, the data was processed using a program called ‘EDWin’, which determines the relationship between depth of focus and exposure latitude.

Some examples of 0.15 µm dense and isolated are shown in Figures 21 and 22. Table 8 gives a tabular summary for a number of differing feature sizes.

All depth of focus and exposure latitude numbers quoted are for the maximum obtained. Cross sections through focus for some of these process windows are shown in Figures 23, 24 and 25.

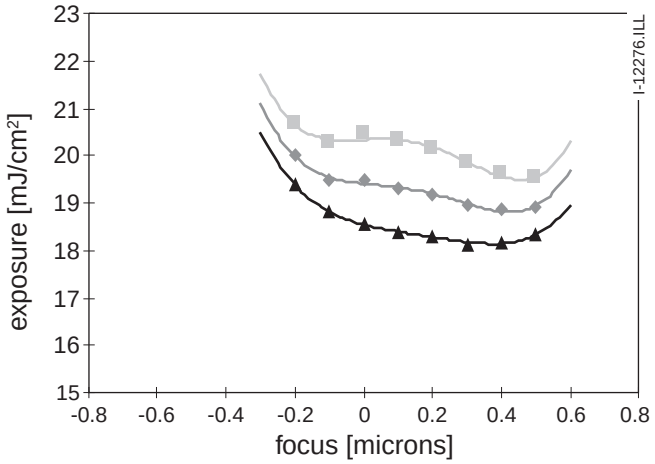

Figure 21 Exposure dose window, 0.15 µm dense lines and spaces

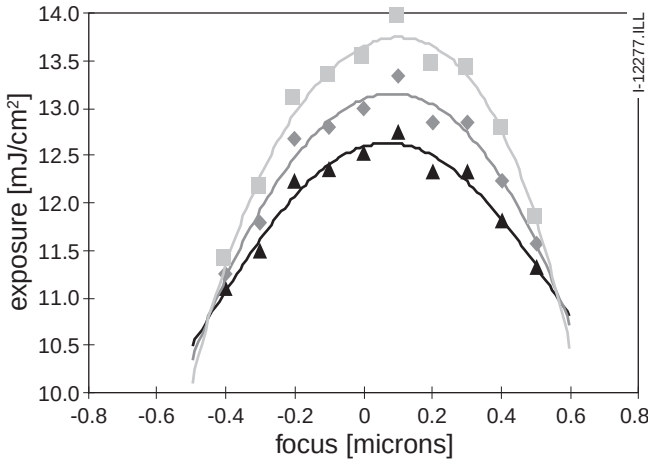

Figure 22 Exposure dose window, 0.15 µm isolated lines

Table 8 Depth of focus (DoF) and exposure latitude (EL) figures for differing feature sizes and differing illumination conditions

CD (µm)	NA = 0.6 σ = 0.85		NA = 0.58 σ = 0.8/0.5		NA = 0.63 σ = 0.8/0.5	
	DoF (µm)	EL (%)	DoF (µm)	EL (%)	DoF (µm)	EL (%)
0.16 dense	0.75	12	0.85	14	0.85	14
0.16 isolated	0.70	10	0.65	11	0.65	10
0.15 dense	0.80	10	0.90	9	0.70	10
0.15 isolated	0.75	9	0.65	9	0.65	9
0.14 dense	0.55	12	0.55	8	0.65	11
0.14 isolated	0.75	9	0.60	9	0.60	9
0.12 1:1.5	0.55	9	0.75	10	0.65	8
0.12 isolated	-	-	0.55	7	0.60	6

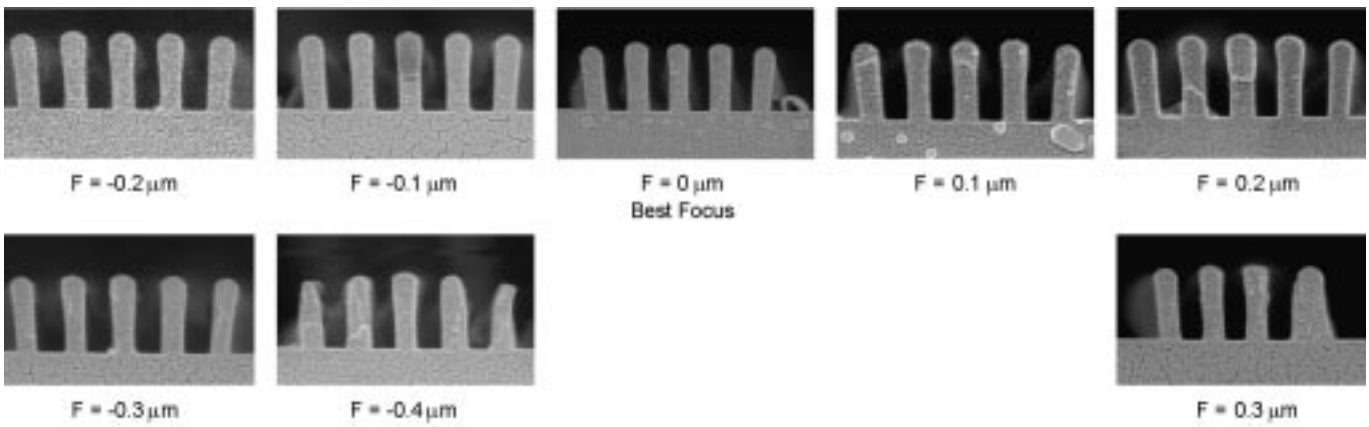

Figure 23 Profiles of 0.13 µm dense lines through focus, OMM ARCH 410/510, NA 0.63, σ_{outer} = 0.8, σ_{inner} = 0.5

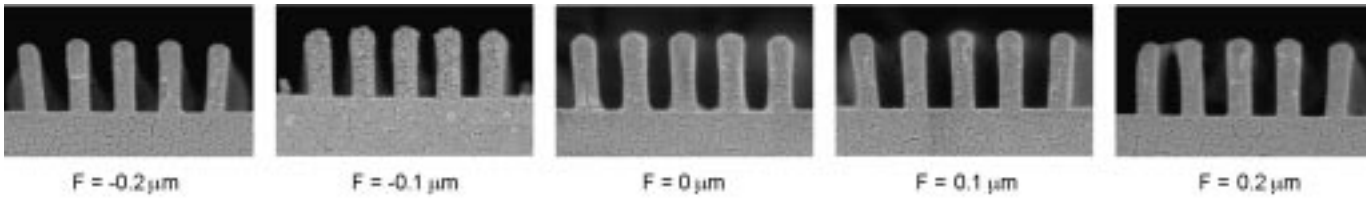

Figure 24 Profiles of 0.13 µm dense lines through focus, OMM ARCH 410/510, NA = 0.60, σ = 0.85

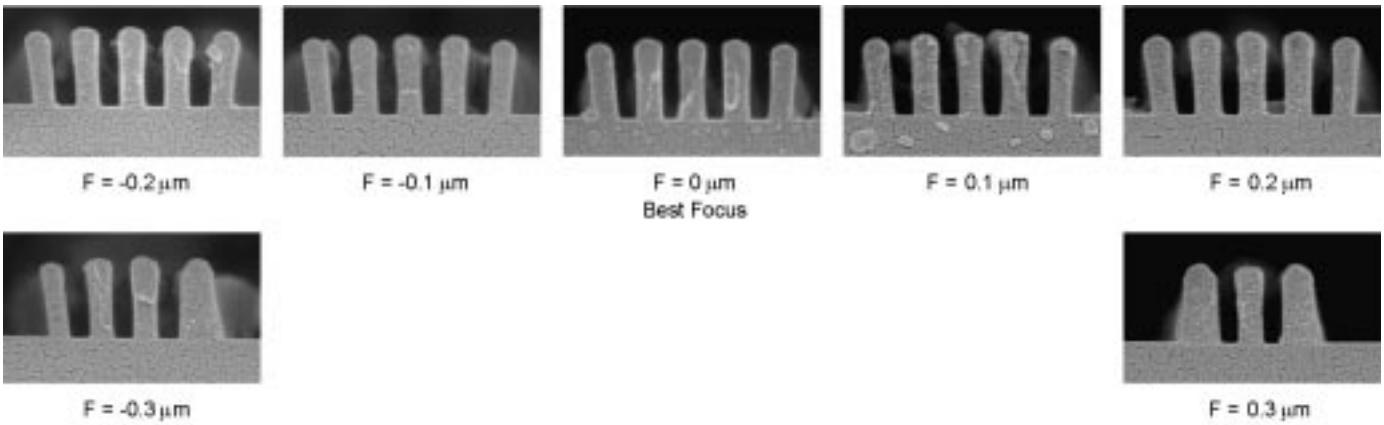

Figure 25 Profiles of 0.12 µm dense lines through focus, OMM ARCH 410/510, NA = 0.63, σ_{outer} = 0.8, σ_{inner} = 0.5

Table 9 Summary of preliminary dense CD uniformity data

	0.16 µm		0.16 µm		0.15 µm		0.14 µm	
	NA = 0.6 σ = 0.85		NA = 0.58, σ = 0.8/0.5		NA = 0.58, σ = 0.8/0.5		NA = 0.58, σ = 0.8/0.5	
	Range	3 σ	Range	3 σ	Range	3 σ	Range	3 σ
CD Uniformity at BF (nm)	19	12	16	11	21	18	19	15
CD Uniformity over 0.4 µm focus range (nm)	27	16	29	15	30	21	32	21

5.6 Full field CD uniformity

As the PAS 5500/900 is a process development/pilot production system, the ability to control CD uniformity is crucial to the successful imaging performance of the system. It is also one of the only tests for fully determining the correct integration of all component subsystems into a working Step & Scan system.

The test used is the standard ASML CD uniformity test where six fields, three focus steps, 20 points in the field, and horizontal and vertical features are analyzed to produce a distribution through focus, averaged over the eighteen fields. The CD uniformity was measured with an automated top down CD SEM and the results have been summarized in Table 9.

5.7 Summary of preliminary CD uniformity data

CD uniformity data may be viewed in many different ways, but two more detailed interpretations of the data are shown in Figures 26 and 27.

Figure 26 shows the distribution of all measurement points in the CD uniformity calculation: horizontal, vertical, -0.2, 0 and +0.2 µm focus steps, totalling 720 CD measurements. It shows two important points: a tight distribution and a negligible horizontal vertical (H-V) CD difference. It is very important to keep this H-V difference as small as possible for CD uniformity issues. There are however many factors which may cause problems here, such as Step & Scan system setup, reticle variations and SEM metrology issues. The results indicate that all possible causes of error are under control.

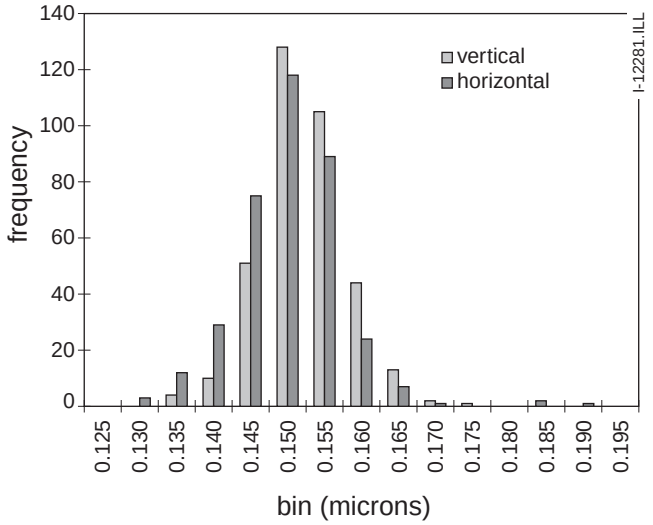

Figure 26 Full field CD uniformity distribution for 0.15 µm dense lines
NA = 0.58, σ = 0.8/0.5

Figure 27 shows a contour plot of the intrafield CD uniformity, measured for 0.14 µm dense lines. The characteristic shape of the plot is probably due to the reticle finger print rather than the system finger print.

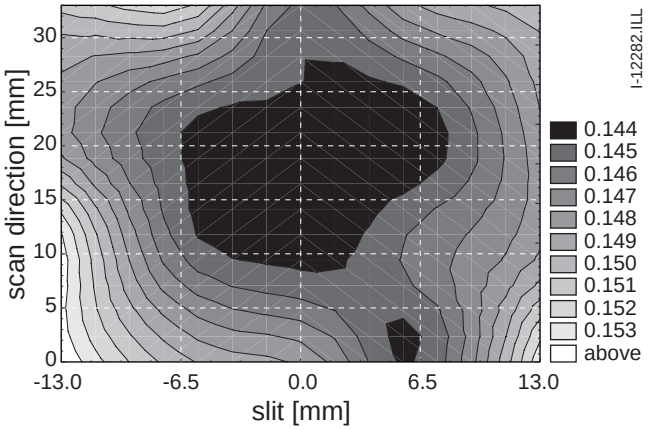

Figure 27 Full field CD uniformity. Intrafield 0.14 µm dense lines
NA = 0.58, σ = 0.8/0.5

5.8 Throughput

The throughput of a system has important influences on the cost of ownership calculations which are discussed in section 6. Throughput is affected by many variables, such as illumination intensity, system transmission and resist sensitivity.

Figure 28 shows the throughput values of the PAS 5500/900 system for different resist sensitivities. The throughput evaluation is determined for a job in which each 200 mm wafer is exposed with 46 fields of 16 mm x 32 mm die size. The values are given for both conventional and annular illumination mode.

With a dose of 10 mJ/cm^2, the PAS 5500/900 produces approximately 60 wafers per hour.

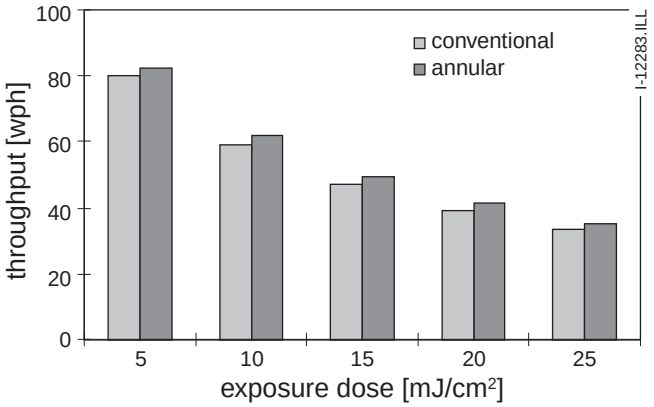

Figure 28 PAS 5500/900 wafer throughput

6. 193 nm TECHNOLOGY AND COST OF OWNERSHIP

6.1 Optical materials and system design

One of the challenging aspects related to 193 nm lithography is the question ‘How do we deal with the performance of the optical materials’. For optical design, SiO_2 and CaF_2 are the only practical candidates. Besides initial quality, radiation induced changes of these glass materials play a role in the resulting system performance.

Fused silica, for example, exhibits compaction as well as radiation-induced absorption. Compaction leads to long term image degradation, whereas induced absorption results in loss of system transmission and wafer throughput.

CaF_2, because it is a crystalline material, does not show compaction nor does it exhibit an induced absorption effect, as we learned from the results of our in-house test marathon. For the illuminator, CaF_2 is the material of choice, it maximizes both transmission and component life time.

For lithographic lenses, CaF_2 is considered a new material, the initial quality of which influences the lens quality. Incorporating CaF_2 in the projection lens relaxes the bandwidth requirements for the ArF

excimer laser, which facilitates the design of high-power line-narrowed lasers, and thus indirectly results in a system with a potentially high wafer throughput.

The PAS 5500/900 Step & Scan system optics are designed in such a way that both optics lifetime and optical efficiency are maximized. For the illumination optics, this means that the optical path through the material has been minimized, whereas the use of CaF_2 has been maximized (especially in those locations with the highest energy density).

To correct for possible induced effects in uniformity or dose control, automated correction mechanisms have been implemented. In the design of the projection lens, the amount of CaF_2 has been balanced between obtaining a maximum bandwidth and a minimum amount of CaF_2. The chromatic aberrations of the resulting lens design have been corrected for a laser bandwidth up to 0.7 pm.

6.2 Litho-cell cost of ownership

The exposure system related aspects in the litho-cell cost of ownership originate from three aspects:

- initial system costs,
- wafer throughput,
- system operating cost.

Because of the limitations in material life time, initial system costs especially have the attention of the 193 nm community.

We compared the litho-cell cost of an ArF, 0.15 µm binary mask technology to a KrF, 0.15 µm engineered mask technology. Input parameters determining the wafer costs are: fixed costs such as capital costs of the exposure system and track, and variable costs for photoresist, reticles, laser and Step & Scan system operating costs.

One of the main contributors to the overall cost of ownership is the cost of reticles. Assuming that 0.15 µm KrF technology implies the use of expensive proximity-corrected phase shift masks, the cost of ownership is expected to rise significantly compared to 0.25 µm KrF technology. The alternative technology, using ArF in combination with a binary mask, might be cheaper, despite the higher laser and optics maintenance costs. Using the reticle cost estimation as presented in [1], we compared the cost of ownership for two types of user:

- users who run more than 10,000 wafers per reticle,
- users who run less than 1500 wafers per reticle.

The results are presented in Figure 29.

In Figure 30, the evaluation is extended to the main technology nodes varying from 0.25 µm down to 0.1 µm.

It is concluded that, from a cost point of view, the insertion point for ArF differs depending on the type of user. Indeed, high volume reticle consumers are expected to enter the 193 nm era at the 0.15 µm node, whereas low volume reticle consumers will extend 248 nm down to the 0.13 µm technology node.

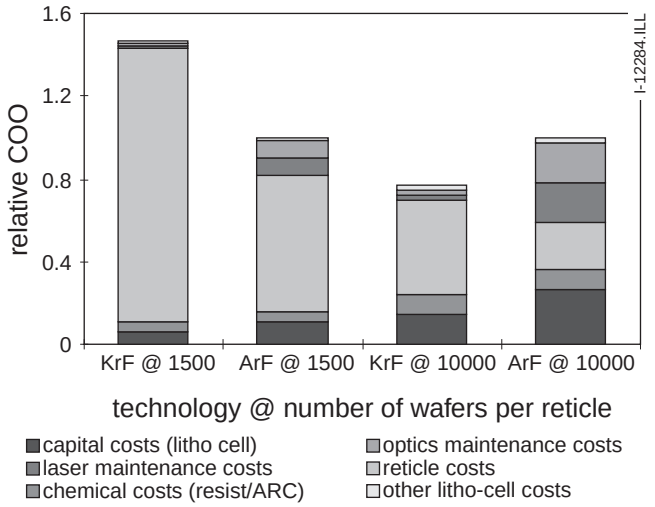

Figure 29 Cost of ownership (COO) comparison of 0.15 µm technology using ArF/binary mask or KrF/phase shift mask

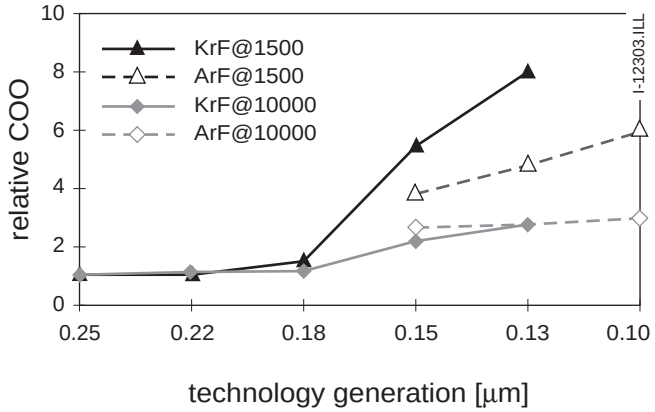

Figure 30 Cost of ownership trend analysis for KrF / phase shift mask and ArF / binary mask technology

7. CONCLUSIONS

The performance of the ASML PAS 5500/900 193 nm Step & Scan system has been demonstrated at both system and subsystem level. Good CD uniformity, excellent distortion and overlay have been shown.

The imaging results presented here are the first results available and show linearity down to 0.14 μm for dense lines and 0.11 μm for isolated features; this is demonstrated on two photoresist processes: OMM ARCH 410/510 and IBM's version 2 photoresist.

Process windows showing acceptable latitudes have been presented. There does, however, appear to be a sizeable iso-dense bias which requires further optimization. Process windows at 0.12 μm show a DoF of 0.4 μm indicating that printing at the SIA 0.13 μm node is possible, although further work to optimize processing and optical conditions is certainly necessary.

Full field CD uniformity data has also been presented to show acceptable full field imaging suitable for pilot production.

Costs of 193 nm lithography will certainly influence the introduction point of this generation of tool but it appears that all the design issues relating to 193 nm lithography have been solved; only improvements in quality and performance now need to be addressed to move from pilot to production worthiness.

The outlook for 193 nm lithography is extremely positive; large improvements are still being made in lasers, quartz and CaF_2, and these will continue to lead to improvements in performance and cost of ownership calculations. It is the improvement in areas as these which will allow 193 nm lithography to approach the 0.10 μm technology node and allow it to be more than a 'one generation tool'.

ACKNOWLEDGEMENTS

Part of this work is funded by the European Community through Esprit project 25434 (ELLIPSE).

The authors would also like to thank all the members of the PAS 5500/900 project at ASML as well as members of the process and SEM group for their continuing support.

The work of Ingrid Pollers and Patrick Janaen of IMEC is also acknowledged here.

Many thanks also to the Zeiss project team and the support of the laser suppliers Lambda Physik and Cymer.

References

[1] W.J. Trybula, P. Seidel, W. Smith and R. L. Engelstad, *Analysis of Future Lithography Masks*, Future Fab International, Vol. 5 1998, pp 195-202.

4022 502 94096